Magnetically-targetable outer-membrane vesicles for sonodynamic eradication of antibiotic-tolerant bacteria in bacterial meningitis

Shi, Rui; Lv, Rui; Dong, Ziliang; Cao, Qinghua; Wu, Renfei; Liu, Sidi; Ren, Yijin; Liu, Zhuang; van der Mei, Henny C.; Liu, Jian

Published in:
Biomaterials

DOI:
10.1016/j.biomaterials.2023.122320

Publication date:
2023

Biomaterials 302 (2023) 122320

Contents lists available at ScienceDirect

Biomaterials

journal homepage: www.elsevier.com/locate/biomaterials

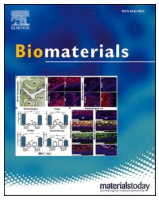

Magnetically-targetable outer-membrane vesicles for sonodynamic eradication of antibiotic-tolerant bacteria in bacterial meningitis

Rui Shi [a,b,1], Rui Lv [a,1], Ziliang Dong [a,c,1], Qinghua Cao [a], Renfei Wu [a,b], Sidi Liu [a,b], Yijin Ren [d], Zhuang Liu [a], Henny C. van der Mei [b,*], Jian Liu [a,**], Henk J. Busscher [b]

[a] Institute of Functional Nano & Soft Materials (FUNSOM), Jiangsu Key Laboratory for Carbon-Based Functional Materials & Devices, Soochow University, 199 Ren'ai Rd, Suzhou, 215123, Jiangsu, PR China

[b] University of Groningen and University Medical Center Groningen, Department of Biomedical Engineering, Antonius Deusinglaan 1, 9713 AV, Groningen, the Netherlands

[c] Science and Technology Innovation Center, Shandong First Medical University, Jinan, 250000, Shandong, PR China

[d] University of Groningen and University Medical Center of Groningen, Department of Orthodontics, Hanzeplein 1, 9700 RB, Groningen, the Netherlands

ARTICLE INFO

Keywords:
Antibiotics
Blood-brain barrier
Membrane vesicles
Meningitis
Recurrence
Sonodynamic therapy

ABSTRACT

Treatment of acute bacterial meningitis is difficult due to the impermeability of the blood-brain barrier, greatly limiting the antibiotic concentrations that can be achieved in the brain. *Escherichia coli* grown in presence of iron-oxide magnetic nanoparticles secrete large amounts of magnetic outer-membrane vesicles (OMVs) in order to remove excess Fe from their cytoplasm. OMVs are fully biomimetic nanocarriers, but can be inflammatory. Here, non-inflammatory magnetic OMVs were prepared from an *E. coli* strain in which the synthesis of inflammatory lipid A acyltransferase was inhibited using CRISPR/Cas9 mediated gene knockout. OMVs were loaded with ceftriaxone (CRO) and meso-tetra-(4-carboxyphenyl)porphine (TCPP) and magnetically driven across the blood-brain barrier for sonodynamic treatment of bacterial meningitis. ROS-generation upon ultrasound application of CRO- and TCPP-loaded OMVs yielded similar ROS-generation as by TCPP in solution. *In vitro*, ROS-generation by CRO- and TCPP-loaded OMVs upon ultrasound application operated synergistically with CRO to kill a hard-to-kill, CRO-tolerant *E. coli* strain. In a mouse model of CRO-tolerant *E. coli* meningitis, CRO- and TCPP-loaded OMVs improved survival rates and clinical behavioral scores of infected mice after magnetic targeting and ultrasound application. Recurrence did not occur for at least two weeks after arresting treatment.

1. Introduction

Acute bacterial meningitis is a life-threatening condition [1,2]. Although vaccination has reduced the incidence of community-acquired meningitis, vaccine-escape by bacterial pathogens frequently occurs [3,4] and mortality amongst meningitis patients still amounts 30% [5] despite extensive antibiotic therapy, while about 9% of all patients have a recurrent meningitis [6]. The failure of antibiotic therapy is first of all due to the impermeability of the blood-brain barrier in the central nervous system [1,7], possessing a unique barrier selectivity. The selectivity of the blood-brain barrier is achieved by small capillaries composed of vascular endothelial cells and surrounded by pericytes and astrocytes. As a result of this selectivity, transport of antibiotics into the cerebrospinal fluid is low and antibiotic concentrations remain below the minimum inhibitory and bactericidal concentration [8,9]. Secondly, innate immune clearance in the central nervous system is poor [10,11]. As a combined result of low antibiotic concentrations and poor immune clearance, infecting bacteria can stop growing and adapt a low metabolic activity to become temporarily antibiotic-tolerant. Antibiotic-tolerant bacteria survive antibiotic treatment and are therewith responsible for recurrence of infection after disappearance of clinical symptoms [12,13]. Although the antibiotic tolerance is initially phenotypic, genotypically tolerant strains, i.e. permanently tolerant strains, have also been found associated with recurrent meningitis [14,15]. Despite the seriousness of meningitis and progress of our understanding of its etiology, it is sobering to read that recent reviews still

* Corresponding author.
** Corresponding author.
E-mail addresses: h.c.van.der.mei@umcg.nl (H.C. van der Mei), jliu@suda.edu.cn (J. Liu).
[1] These authors contributed equally to this work.

https://doi.org/10.1016/j.biomaterials.2023.122320
Received 10 July 2023; Received in revised form 6 September 2023; Accepted 9 September 2023
Available online 17 September 2023

conclude that the physicochemical properties of antimicrobials are not well suited to cross the blood-brain barrier and accordingly alternative treatment strategies are still direly needed [3,16,17].

Sonosensitizers [18,19] generate reactive oxygen species (ROS) upon low-frequency ultrasound activation, operating synergistically with antibiotics [20,21]. Moreover, sonodynamic therapy exhibits high tissue penetration and negligible tissue damage as compared with photodynamic therapy [20,22]. Sonodynamic therapy has not yet been applied for the treatment of bacterial meningitis due to the difficulties involved in transporting sonosensitizers and antibiotics across the blood-brain barrier.

Extracellular Outer-Membrane Vesicles (OMVs) constitute a fully biomimetic nanocarrier. OMVs are secreted by various cell types, amongst which Gram-negative and Gram-positive bacterial strains. OMVs by nature serve to transport proteins, DNA, signaling molecules and toxins over long distances through the blood circulation [23,24]. Low harvesting yields of OMVs have hitherto impeded their use as a clinically applicable drug nanocarrier. Besides, OMVs can be highly inflammatory [25]. Making use of the natural ability of bacteria to secrete OMVs to remove excess Fe from their cytoplasm, we have recently described how Gram-negative *Escherichia coli*, grown in the presence of iron-oxide magnetic nanoparticles can be induced to secrete high amounts of OMVs with internalized iron-oxide magnetic nanoparticles [26]. Internalization of magnetic nanoparticles during bacterial growth was demonstrated using transmission electron microscopy and high-angle annular dark-field scanning transmission electron microscopy with elemental mapping, while inductively coupled plasma-mass spectrometry showed an iron uptake of around 7 μg/10^9 bacteria. This facilitated high yield, magnetic harvesting of these OMVs. Magnet harvesting yields were found to be up to 60 times higher than yields obtained using traditional methods, such as ultrafiltration [27] or OMV-coating of nanoparticles by co-extrusion [28], which brings the use of OMVs considerably closer to clinical application. Moreover, magnetically harvested OMVs can be driven into an infectious biofilm using an externally applied magnetic field [26].

The current study aimed to test our hypothesis that due to their above described biomimicry, magnetically harvested OMVs secreted by *E. coli* grown in presence of iron-oxide magnetic nanoparticles can be loaded with an antibiotic and a sonosensitizer and driven across the blood-brain barrier using an externally applied magnetic field for the treatment of bacterial meningitis. In order to test this hypothesis and prevent inflammation upon *in vivo* use of bacterial OMVs, we first constructed an *E. coli* Δ*msbB* mutant in which lipid A acyltransferase is synthesized possessing a modified lipid A structure which reduces the inflammatory response against the *E. coli* OMVs secreted [25]. Subsequently, non-inflammatory, magnetically harvested OMVs were sonically loaded with ceftriaxone (CRO; an antibiotic used in the clinical treatment of meningitis) and loaded by incubation with meso-tetra-(4-carboxyphenyl)porphine (TCPP; a potent sonosensitizer). First absence of inflammatory responses and biosafety of CRO- and TCPP-loaded magnetic OMVs were established in mice, after which anti-bacterial efficacy of CRO- and TCPP-loaded magnetic OMVs were determined in vitro, against a hard-to-kill, CRO-tolerant *E. coli*. Finally, a murine meningitis model was used to demonstrate that CRO- and TCPP-loaded magnetic OMVs could be magnetically driven across the blood-brain barrier to facilitate highly effective sonodynamic treatment of bacterial meningitis.

2. Results

2.1. Preventing inflammatory effects upon OMV injection

Prevention of inflammatory effects is crucial for any potential human application of OMVs. In order to prevent inflammation upon *in vivo* use of bacterial OMVs, an *E. coli* mutant was constructed via CRISPR/Cas9 mediated gene knockout to inactivate lipid A acyltransferase synthesis [29]. Knockout of *msbB* genes in *E. coli* MG1655 Δ*msbB*, responsible for lipid A acyltransferase synthesis, was demonstrated using agarose gel electrophoresis (Fig. 1A). OMVs from the knock-out strain *E. coli* MG1655 Δ*msbB*, did not invoke a response to infection of RAW 264.7 macrophages, opposite to OMVs from wild-type *E. coli* MG1655 (see Fig. S1).

Subsequently, OMVs were magnetically harvested (see Fig. 1B) from the *E. coli* MG1655 parent and the *E. coli* MG1655 Δ*msbB* mutant strain and loaded with CRO and TCPP (see section below). When *E. coli* MG1655 derived magnetic OMVs were injected in mice at a dose of 6 mg/kg body, all mice in a group of 8 died within 48 h after injection. Oppositely, all mice injected with a ten-fold higher dose of 60 mg/kg of magnetic OMVs derived from the Δ*msbB* mutant survived (Fig. 1C). In a group of mice injected with a low, non-lethal dose of 0.6 mg/kg of *E. coli* MG1655 derived OMVs (see also Fig. 1C), significantly increased serum levels of IL-6 and TNF-α relative to PBS were found (Fig. 1D). Injection of this low, non-lethal dose of *E. coli* MG1655 Δ*msbB* derived OMVs on the other hand, yielded similarly low serum levels of IL-6 and TNF-α, as observed upon injection of PBS (see Fig. 1D). Collectively, these data confirm absence of inflammatory lipid A acyltransferase in CRO- and TCPP-loaded OMVs derived from *E. coli* MG1655 Δ*msbB*.

Biosafety of intravenous injection in mice of CRO- and TCPP-loaded magnetic, non-inflammatory OMVs derived from *E. coli* MG1655 Δ*msbB* was further examined based on blood biochemistry (Fig. S2A), cell counts (Fig. S2B) and histological analysis of major organ tissues (Fig. S2C). Blood biochemistry and cell counts did not show any abnormalities up to at least 15 days after intravenous injection (Fig. S2A and **S2B**). Also, neither heart, kidney, spleen, lung nor liver tissues of mice, sacrificed 1, 7 or 15 days after injection, demonstrated signs of inflammation (Fig. S2C) Collectively, these results indicate that magnetic, non-inflammatory OMVs derived from *E. coli* MG1655 Δ*msbB* remained biosafe upon loading of CRO and TCPP.

2.2. CRO- and TCPP-loading and release from OMVs upon ultrasound application

Next, *E. coli* MG1655 Δ*msbB* derived magnetic OMVs were sonically loaded with CRO, while TCPP was loaded upon incubation with OMVs (see also Fig. 1B). Loading increased with increasing concentrations of CRO (Fig. S3A, B and **S4A**) and TCPP (Fig. S3C, D and Fig. S4B) in solution up to maximal levels using 1500 μg/mL CRO and 200 μg/mL TCPP. Hence, concentrations of 1500 μg/mL CRO and 200 μg/mL TCPP were further employed for the loading of magnetically derived OMVs in the remainder of this study.

Mass spectroscopy indicated peaks at *m/z* equal to 577.8 and 791.5 (Fig. 2A), indicative of CRO and TCPP, respectively. Subsequently, loading contents of CRO and TCPP were calculated based on UV absorbances (Fig. S3) and found to be 590 and 128 ng/μg of OMV protein for CRO and TCPP, respectively (roughly equivalent with 7.7×10^{-7} ng CRO and 1.7×10^{-7} ng TCPP per OMV).

OMV diameters did not increase upon loading of CRO and TCPP and hovered around 115 nm (Fig. 2B), while a spherical morphology remained to exist (Fig. 2C). This demonstrates absence of any impact on the integrity after loading, neither by cavitation and microstreaming during CRO loading, nor by distribution in the lipid bilayer and diffusion of hydrophobic TCPP into the OMVs. Zeta potentials of magnetic OMVs did not significantly change upon loading (Fig. 2D) due to the negative charge of TCPP [30]. CRO- and TCPP-loaded magnetic OMVs had diameters and zeta potentials that remained stable up to at least 9 days in PBS (Fig. 2E).

CRO and TCPP release from OMVs in absence of ultrasound application increased with time to level off after 12 h around 20% (Fig. 3A), presumably by diffusion through OmpF porins in OMVs [31]. Cavitation and microstreaming during ultrasound application in the vicinity of the OMVs may lead to a disruption of their membrane structure [32,33]. Accordingly, only 5 min application of ultrasound enhanced release of

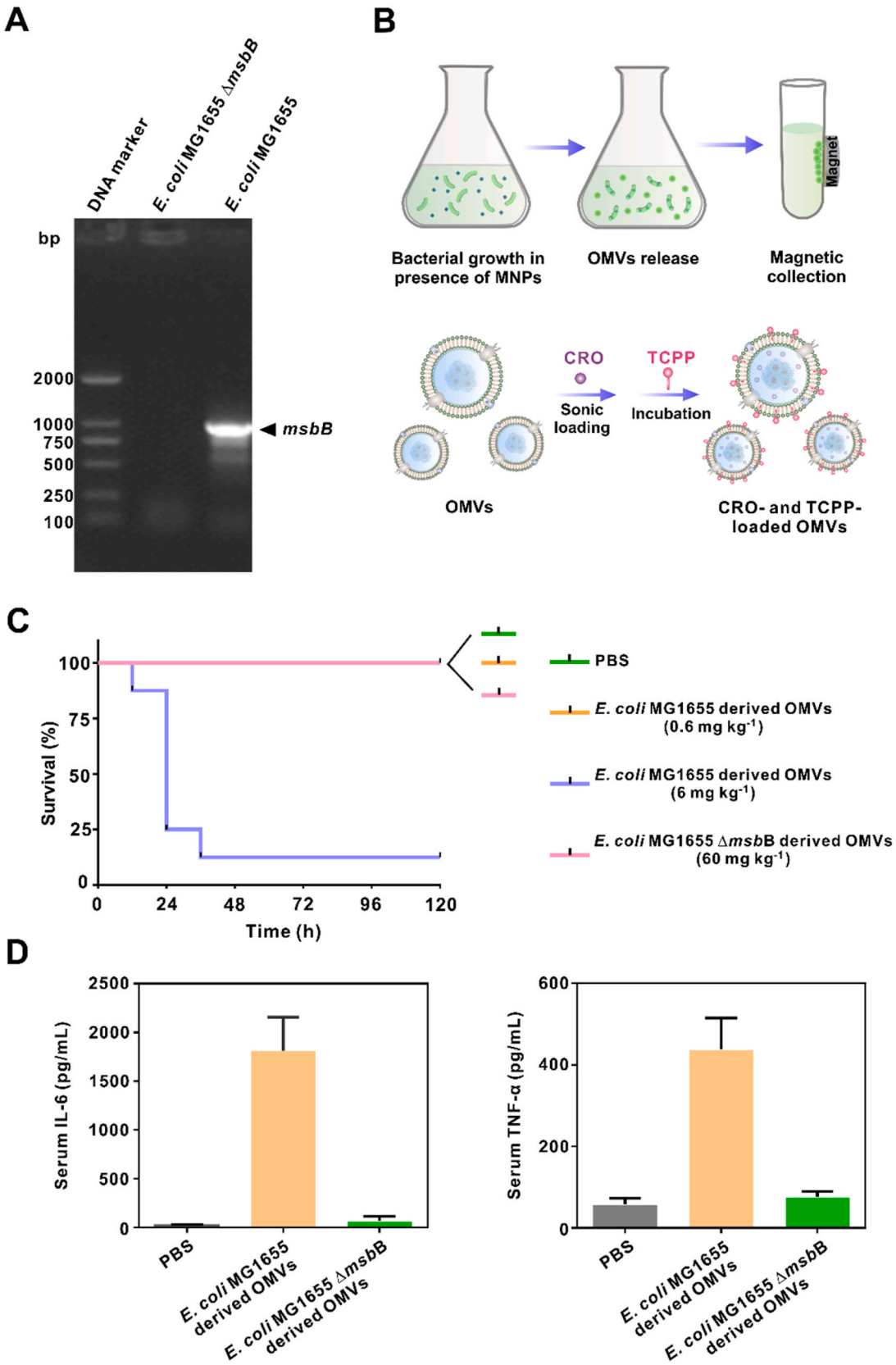

Fig. 1. Construction of a non-inflammatory *E. coli* mutant and magnetic harvesting of OMVs. **(A)** Agarose gel electrophoresis, demonstrating absence of *msbB* genes in *E. coli* MG1655 after CRISPR/Cas9 knockout. **(B)** Magnetic harvesting of OMVs secreted by *E. coli* grown in presence of iron-oxide magnetic nanoparticles and loading of CRO and TCPP. **(C)** Survival rates of mice intravenously injected with PBS or different doses of CRO- and TCPP-loaded magnetic OMVs (n initially equals 8 mice per group). **(D)** IL-6 and TNF-α levels in serum, taken from mice, 6 h after intravenous injection mice with 100 μL PBS, *E. coli* MG1655 or *E. coli* MG1655 Δ*msbB* derived magnetic OMVs (dose: 0.6 mg/kg). Data in all panels represent means ± SDs over triplicate experiments with groups of 3 mice.

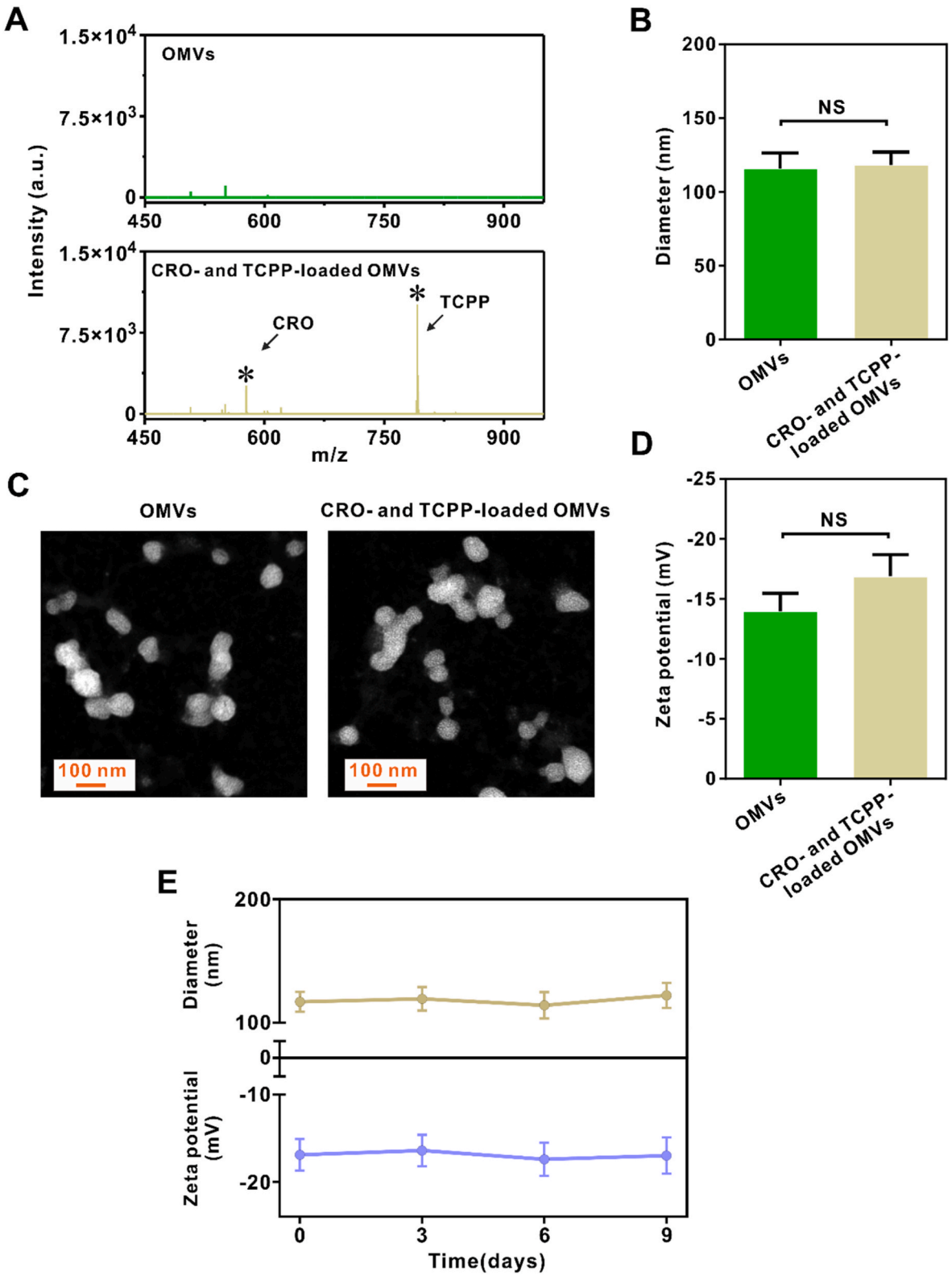

Fig. 2. CRO- and TCPP-loading of OMVs, OMV diameters and zeta potentials. **(A)** Mass spectrometry of magnetic OMVs in absence (top figure) and presence of CRO- and TCPP-loading (bottom figure). **(B)** Hydrodynamic diameters of magnetic OMVs in absence and presence of CRO- and TCPP-loading, measured in PBS (pH 7.4). **(C)** HAADF-STEM micrographs of OMVs in absence and presence of TCPP- and CRO-loading. **(D)** Same as panel (b), now showing OMV zeta potentials. **(E)** Stability of magnetic OMVs loaded with CRO and TCPP in PBS (pH 7.4) at 25 °C as a function of time. Data in all relevant panels represent means ± SDs over triplicate experiments with separate batches of OMVs. NS indicates absence of statistical significance at $p > 0.05$ (Student's t-test).

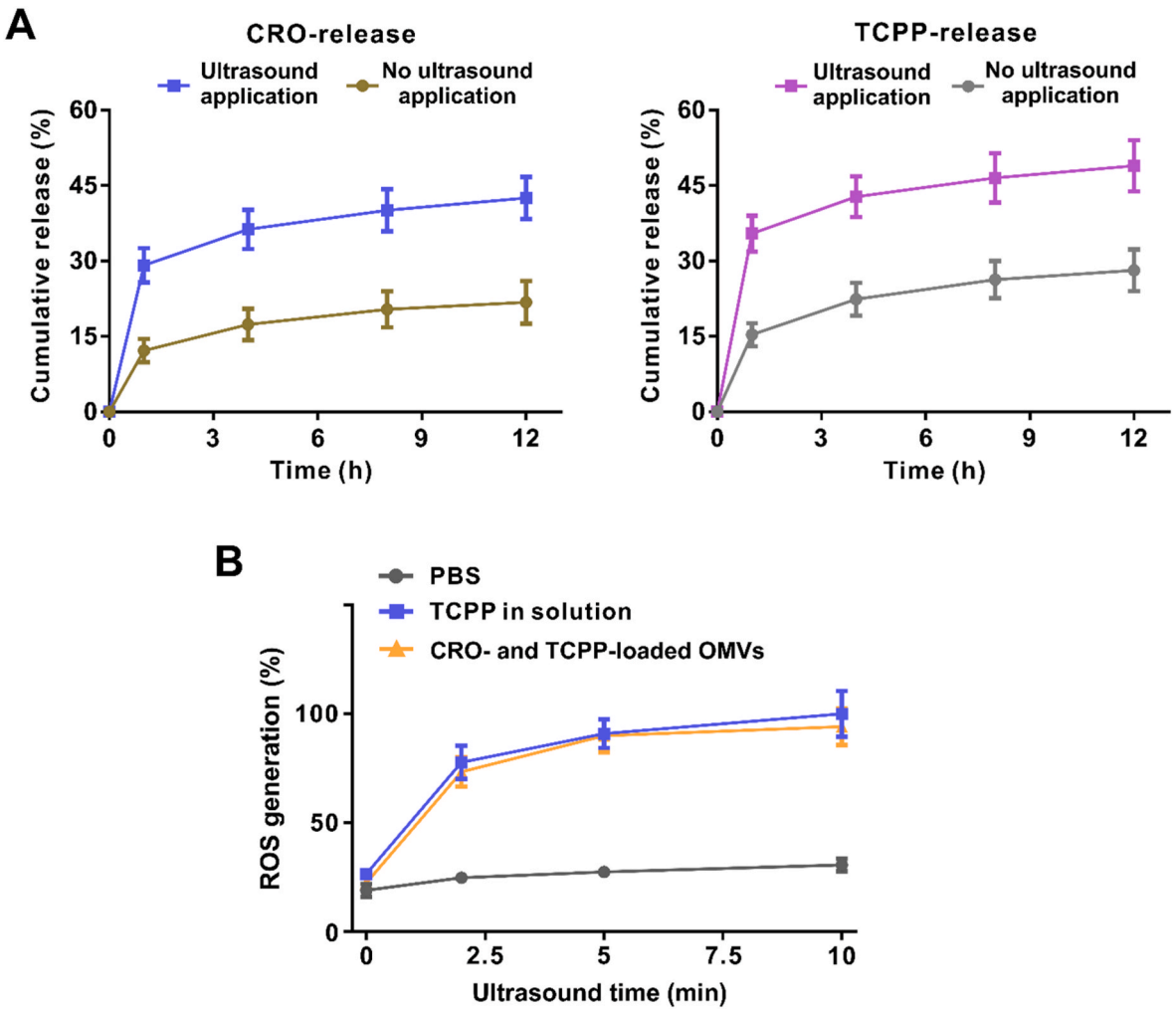

Fig. 3. Release of CRO and TCPP from OMVs after ultrasound application (40 kHz, 2 W/cm^2, 50% duty cycle) in PBS and ROS generation at a TCPP-equivalent concentration of 2 μg/mL. **(A)** Release of CRO and TCPP from CRO- and TCPP-loaded OMVs as a function of time, starting 5 min after arresting ultrasound application. Release was expressed relative to the amount of CRO and TCPP loaded at time 0, set at 100%. **(B)** ROS generation by TCPP in solution and in CRO- and TCPP-loaded OMVs as a function of time, starting 5 min after arresting ultrasound application. ROS generation was quantitated based on ROS-induced oxidation of singlet-oxygen sensor green (SOSG) into green-fluorescent SOSG endoperoxide [34]. ROS generation was expressed relative to the total amount of ROS generated after 10 min. Data in all panels represent means ± SDs over triplicate experiments with separate batches of OMVs.

CRO and TCPP, now leveling off after 12 h around 45%. Concurrent with ultrasound-enhanced release of TCPP, ROS was generated (Fig. 3B). ROS generation upon TCPP release was not affected by the absence or presence of CRO-loading of OMVs (Fig. 3B).

2.3. Efficacy of CRO- and TCPP-loaded OMVs against CRO-tolerant *E. coli*

CRO-tolerant bacterial strains constitute a major problem in the clinical treatment of meningitis. Therefore, first, a CRO-tolerant *E. coli* strain was constructed, according to a literature procedure [35] by repeated sub-culturing of *E. coli* ATCC 25922 in presence of sub-inhibitory concentrations of CRO (see Fig. S5A). After eight cycles of repeated sub-culturing, the MIC (0.24 μg/mL) had not increased (Fig. S5Band Table S1), while the strain was more slowly killed over time in presence of CRO (Fig. S5C). However, compared with the parent strain, the MBC of the CRO-tolerant strain had increased by a factor of eight, while the minimal duration of exposure to CRO for achieving 99% killing had increased from 2 h to almost 8 h. This is a typical feature of antibiotic-tolerant bacterial pathogens and demonstrates that the *E. coli* strain obtained after repeated sub-culturing in presence of CRO had indeed become CRO-tolerant, regardless of whether *E. coli* were exposed to CRO free in solution or released from OMVs. Note from Table S1 that TCPP either free in solution or released from OMVs did not affect the viability of the *E. coli* parent strain nor of its CRO-tolerant mutant, regardless of ultrasound application.

CRO- and TCPP-loaded OMVs as well as OMVs loaded only with CRO, both reduced the number of *E. coli* CFUs in suspension by 2 log units in absence of ultrasound application (Fig. 4A). OMVs loaded with only TCPP did not cause any decrease in CFUs as compared with a bacterial suspension in PBS, regardless of ultrasound application. Application of ultrasound did not further contribute to *E. coli* killing in suspension by CRO- or TCPP-loaded OMVs. However, *E. coli* killing upon ultrasound application by CRO- and TCPP-loaded OMVs yielded 1.5 log units larger killing than by OMVs single-loaded with CRO, i.e. 3.5 log units better killing than achieved in PBS. This points to synergistic killing by CRO and the ROS generated upon ultrasound application to TCPP.

ROS generation in *E. coli* after exposure to CRO- and TCPP-loaded OMVs was confirmed using bacteria stained with 2′,7′-dichlorodihydrofluorescein (DCFH-DA), demonstrating green-fluorescence in presence of ROS [34]. Green-fluorescence *E. coli* were virtually absent in presence of OMVs without ultrasound application, but after exposure to CRO- and TCPP-loaded OMVs and ultrasound application the majority of

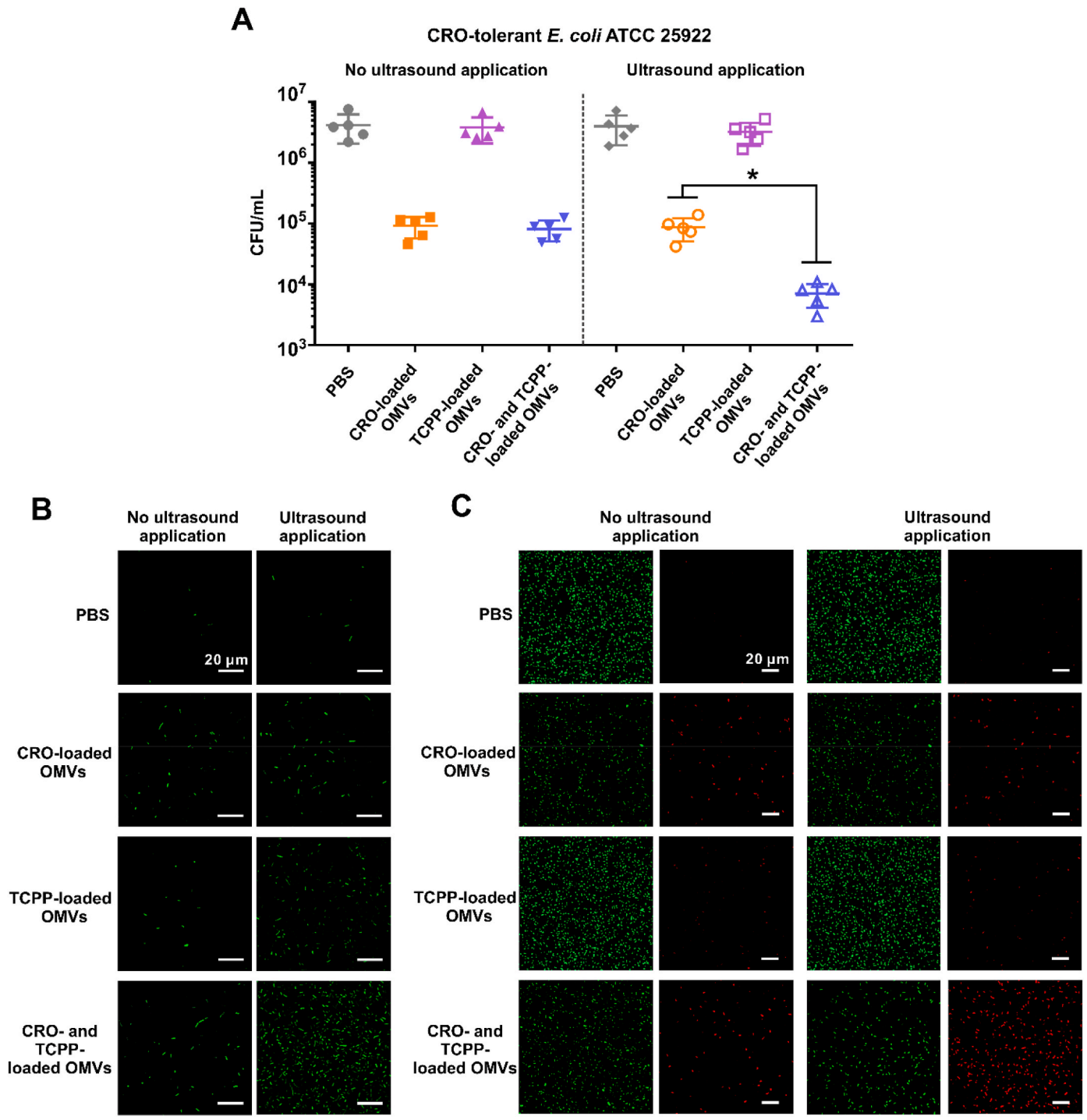

Fig. 4. *In vitro* antibacterial effects of CRO- and TCPP-loaded magnetic OMVs against planktonic, CRO-tolerant *E. coli* ATCC 25922 after 5 min ultrasound application. 1 mL of an *E. coli* suspension in PBS at pH 7.4 (5×10^6 bacteria/mL) was mixed for 2.5 h with CRO-, TCPP- or CRO- and TCPP-loaded OMVs (CRO and TCPP equivalent concentrations in all experiments amount 2 μg/mL and 0.4 μg/mL, respectively). For CLSM imaging, suspensions were concentrated to 10^8 bacteria/mL after treatment. **(A)** The number of CFUs of CRO-tolerant *E. coli* after exposure to OMVs in absence or after ultrasound application. Error bars denote standard deviations over 5 measurements with separately prepared batches of OMVs and different bacterial cultures. * indicates significant differences at $p < 0.05$ between data indicated by the spanning bars (one-way ANOVA). **(B)** Presence of intracellular ROS inside *E. coli* in PBS after *E. coli* staining with a green-fluorescence ROS probe (DCFH-DA) [34]. **(C)** Cell wall damage in *E. coli* in PBS after staining with SYTO9/propidium iodide. Cell wall damage turns green-fluorescent bacteria into red-fluorescent ones [36].

bacteria showed green-fluorescence in CLSM images (Fig. 4B). Minor ROS generation was observed in case *E. coli* were exposed to TCPP-loaded OMVs after ultrasound application. Concurrently, severe cell wall damage, visualized by red-fluorescent *E. coli* after SYTO9/-propidium iodide staining, only occurred upon exposure to CRO- and TCPP-loaded OMVs after ultrasound application (Fig. 4C). Importantly, ROS generation upon ultrasound application did not affect the viability of human umbilical vein endothelial cells (see Fig. S6). Collectively, these observations point to a synergy between CRO and TCPP in the sonodynamic killing of CRO-tolerant *E. coli*, as supported by the absence

of sonodynamic bacterial killing in the presence of a ROS scavenger (thiourea; see Fig. S7).

2.4. Magnetically-driving OMVs across the blood-brain barrier in mice and removal from the body

Fluorescence imaging demonstrated that TCPP in solution was unable to cross the blood-brain barrier after tail-vein injection, regardless of magnetic field application on top of the head of the mice (Fig. 5A). Similarly, TCPP was not detected in the brains of mice when loaded together with CRO in magnetic OMVs in absence of magnetic field application, but TCPP was detected in the brain within 1 h after tail-vein injection upon application of a magnetic field at a dose of 50 mg/kg, known to be safe for use in neonates [37]. Quantitative analysis of the red-fluorescence as a function of time after tail-vein injection of TCPP-loaded OMVs and magnetic field application, showed a steady increase in red-fluorescence in the brain due to TCPP accumulation that reached a maximum after 3 h (Fig. 5B).

In order to study the distribution of OMVs within the brain, mice were sacrificed 3 h and 24 h after tail-vein injection of OMVs and magnetic field application, after which brain sections were taken and stained for microscopic analyses. Three hours after injection, red-fluorescent OMVs could be found outside of the vasculature, both in the ventricular and cortical regions of the brain (Fig. 5C). Few red-fluorescent OMVs had remained detectable in the brains of mice sacrificed 24 h after injection. Besides accumulation in the brain after magnetic field application, magnetic OMVs were found accumulated in the liver, spleen, lungs and kidneys of mice due to convective-diffusion through the blood circulation (Fig. 5D). After 24 h however, accumulation had significantly decreased compared to 3 h in all organs, including the brains with exception of the kidneys (see also Fig. 5D), where no significant decrease in fluorescence was observed. Collectively, these data indicate that CRO- and TCPP-loaded magnetic OMVs can be magnetically-driven across the blood-brain barrier to reach an infection site and are removed from the brain and the body by natural processes through the urinary tract.

2.5. Treatment of bacterial meningitis in mice using magnetic CRO- and TCPP-loaded OMVs

Acute, bacterial meningitis was initiated in mice according to a literature protocol [38,39], by injecting a dose of 1×10^5 CFU/site of CRO-tolerant *E. coli* ATCC 25922 directly into the sub-arachnoid region of the brain. Twelve hours after initiating infection, mice showed minor signs of abnormal behavior (clinical behavior score ≤ 1) as the onset of meningitis. At day 0, mice were randomly divided into five groups for treatment with PBS, CRO free in solution or magnetic OMVs loaded with CRO and TCPP that were magnetically driven across the blood-brain barrier by magnetic field application for 3 h. Magnetic field application was followed by 5 min ultrasound application (see scheme in Fig. 6A). Treatment using CRO- and TCPP-loaded OMVs was also carried out in absence of magnetic field or ultrasound application. Treatment was done at 09.00 a.m. The clinical behavior score was taken 1 h before each treatment at 08.00 a.m. and rapidly increased in mice treated with PBS (Fig. 6B). All mice treated with PBS died (score 4) within 3 days after initiating treatment (Fig. 6C). Similarly, the clinical behavior score of mice treated with CRO free in solution or magnetic CRO- and TCPP-loaded OMVs magnetically-driven across the blood-brain barrier, either in absence of ultrasound application or in absence of magnetic field application, increased to around 3 (unable to walk). After 120 h, only 25%–35% of the mice had survived the above treatments. However, after magnetically driving CRO- and TCPP-loaded OMVs across the blood-brain barrier and upon application of ultrasound, clinical behavior scores remained low to hover around 1 (see also Fig. 6B) and all but five mice survived (75%; see also Fig. 6C). Continued monitoring of the surviving mice showed no further deaths up to 18 days after initiating treatment (Fig. 6C).

In the five different groups of infected mice, randomly-selected mice were sacrificed at day 2 prior to the third treatment to assess bacterial CFUs in the brain. In line with the time course of the clinical behavior of mice, magnetically directed CRO- and TCPP-loaded OMVs after ultrasound application yielded the largest reduction in *E. coli* CFUs in the brain (Fig. 6D). Mice surviving treatment were kept alive for another 14 days after arresting treatment and accordingly sacrificed at day 18 and brain tissue was examined for bacterial regrowth. The number of CFUs in brain tissue had decreased further with respect to the number of CFUs found for all treatments (Fig. 6E). However, 14 days after arresting treatment at day 18, the beneficial effects of treatment with magnetic OMVs loaded with CRO and TCPP followed by magnetic field and ultrasound application were about 20-fold larger than of CRO free in solution or of CRO- and TCPP-loaded OMVs in presence of only magnetic field or ultrasound application. This suggests a smaller chance upon recurrence of infection.

Histological examination of brain sections of mice sacrificed at day 2 after hematoxylin and eosin staining (Fig. 6F), exhibited neutrophils both in the ventricular and meningeal outer regions of the brain, along with thickening of the meningeal layer in mice treated with PBS. Also in mice treated with PBS and CRO free in solution, erythrocytes were massively visible in ventricular and meningeal brain regions. These features were rare or absent in infected animals treated with magnetically-directed TCPP- and CRO-loaded OMVs after ultrasound application. Also, the number of apoptotic cells visualized using TUNEL-staining (Fig. 6G), appeared remarkably reduced in the ventricular and meningeal regions upon treatment with magnetically-directed TCPP- and CRO-loaded OMVs after ultrasound application, demonstrating reduced brain damage.

3. Discussion

The work presented in this article addresses the urgent need expressed in many recent reviews on the treatment of meningitis [3,16,17] to develop antimicrobials with physicochemical properties that allow crossing of the blood-brain barrier. The ease at which magnetic bacterial OMVs can be magnetically harvested in large quantities nowadays [26], has paved the way for advancing the clinical use of OMVs as antimicrobial nanocarriers with different physicochemical properties than all currently known drug carriers. Here we demonstrate that non-inflammatory, magnetic bacterial OMVs loaded with an antibiotic and a sonosensitizer are highly efficacious in the treatment of CRO-tolerant *E. coli* induced meningitis in mice.

Application of CRO- and TCPP-loaded OMVs could be done in mice without causing any demonstrable signs of inflammation (Fig. 1C, D and Fig. S2), due to the use of OMVs harvested from an *E. coli* mutant with knocked out msb genes. Knockout of msb genes, inhibited lipid A acyltransferase synthesis [40,41], yielding production of non-inflammatory, under-acylated LPS by the *E. coli ΔmsbB* mutant, that significantly reduced the immune response to LPS.

Rapid crossing of the blood-brain barrier is achieved by magnetically driving antimicrobial loaded OMVs across the blood-brain barrier in a short period of time without causing demonstrable brain damage (Fig. 6F and **G**). This is in line with multiple *in vivo* studies in animals [33], showing that ultrasound transiently and reversibly opens the blood-brain barrier with barrier function returning to normal within 20 h [42]. Peptide modification of nanoparticles is also under investigation nowadays for crossing the blood-brain barrier [43,44], but mostly relies on convective-diffusion through the blood-circulation and receptor-mediated interactions that are hampered by the formation of a protein corona around the nanoparticles [45]. Relying solely on diffusion-crossing of the blood-brain barrier however, takes too long to rely upon in case of acute meningitis, making fast, magnetic-driving of OMVs across the blood-brain barrier a major advantage above slow diffusion-driven crossing. Importantly, once magnetically driven into

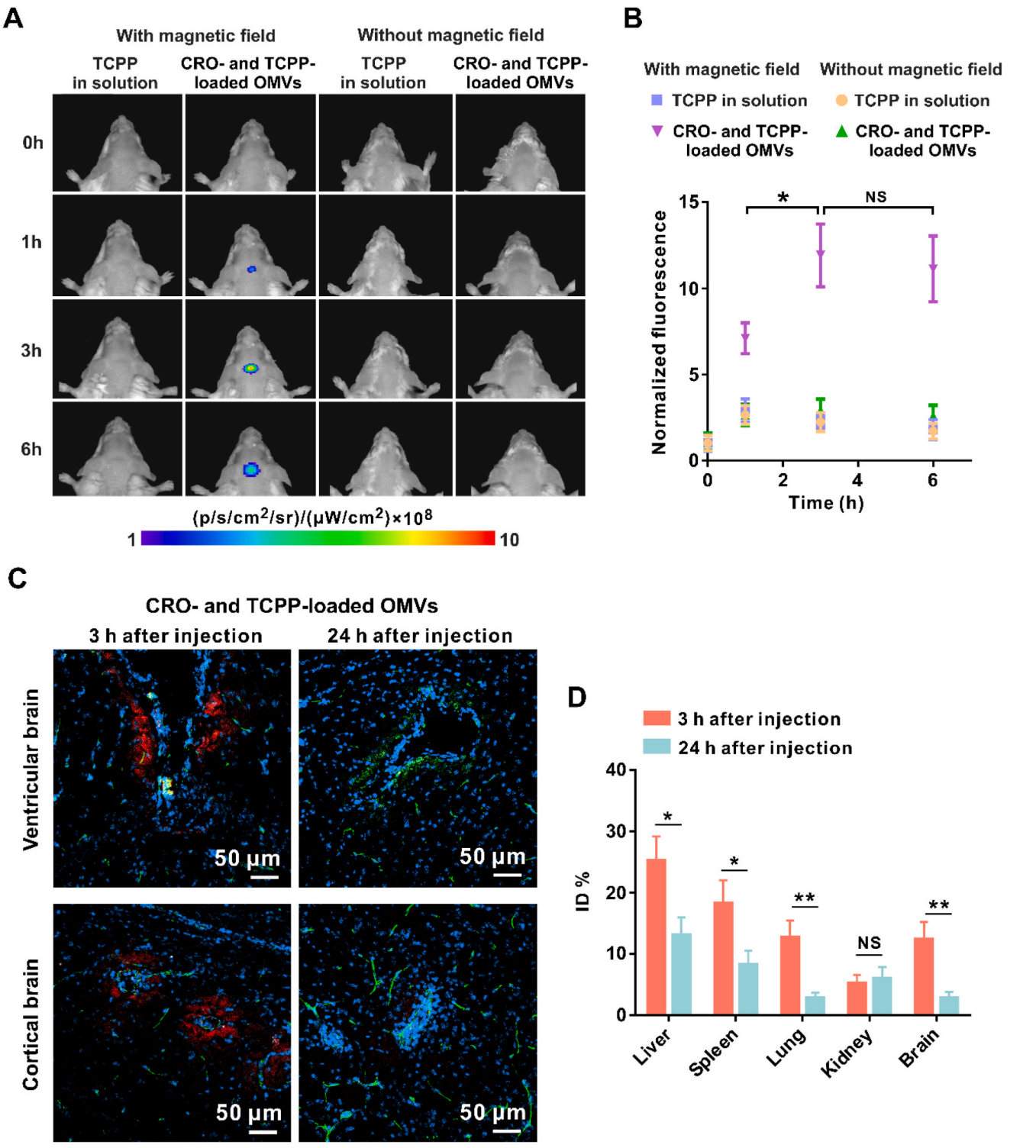

Fig. 5. Magnetically driving CRO- and TCPP-loaded OMVs across the blood-brain barrier in mice. CRO- and TCPP-loaded OMVs (CRO and TCPP equivalent doses amount 50 mg/kg and 10 mg/kg, respectively) and TCPP in solution (10 mg/kg) were tail-vein injected into the vasculature. OMVs were visualized making use of the red-fluorescence of TCPP (emission at 710 nm upon excitation at 660 nm). **(A)** Fluorescence images of mice at different points in time after tail-vein injection in absence and presence of an externally applied magnetic field on top of the head of mice. Magnetic field application was done up to 6 h. Red-fluorescence is presented on a pseudo-color scale. **(B)** Quantification of TCPP red-fluorescence in the brains of mice, as derived from fluorescence images as presented in panel a. **(C)** Distribution of red-fluorescent CRO- and TCPP-loaded OMVs after passing the blood-brain barrier in ventricular and cortical regions of the brain in mice, sacrificed 3 h or 24 h after tail-vein injection of OMVs. Brain sections were stained with green-fluorescent CD31 (vasculature) and blue-fluorescent DAPI (nuclei). **(D)** Distribution of CRO- and TCPP-loaded OMVs in different organs of mice, sacrificed 3 h or 24 h after tail-vein injection of OMVs and expressed as a percentage of the injected dose (ID%), based on the red-fluorescence of TCPP. Data in all panels represent means ± SDs over triplicate experiments within groups of 3 mice. * and ** indicate statistical significances at $p < 0.05$ and $p < 0.01$, respectively. NS means not significant at $p > 0.05$ (one-way ANOVA).

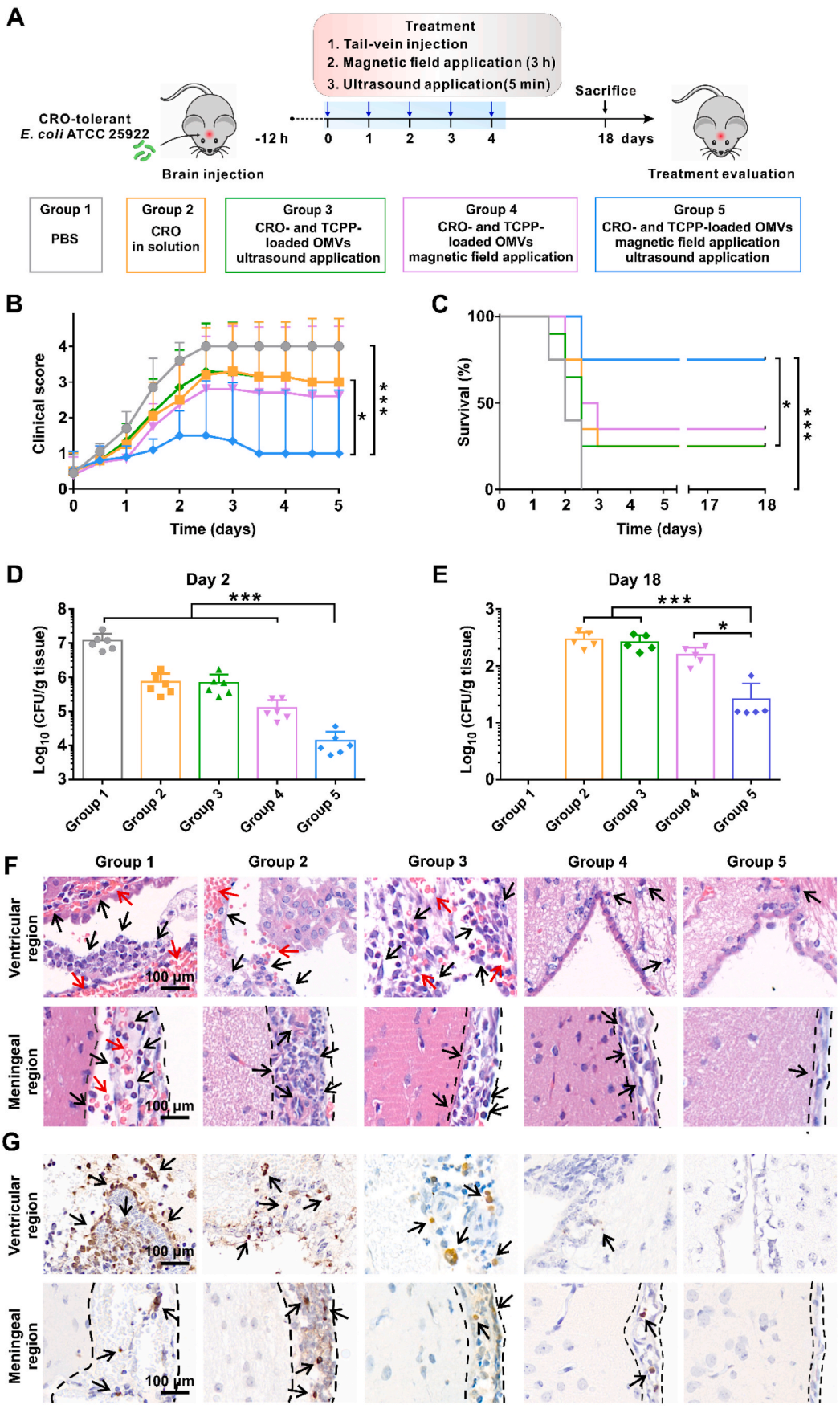

Fig. 6. Treatment of CRO-tolerant *E. coli* ATCC 25922 induced meningitis in a murine model. **(A)** Three-step treatment schedule, starting 12 h after initiation of infection. Treatment involved tail-vein of PBS, CRO free in solution or CRO- and TCPP-loaded OMVs (CRO- and TCPP equivalent doses of 50 mg/kg and 10 mg/kg, respectively). Initially, 20 mice were included in each group. **(B)** Clinical behavior scores of mice with *E. coli* induced meningitis as a function of time after initiating treatment. Data represent means ± SDs over each group. Differences between groups were analyzed using one-way ANOVA. * and *** indicate significant differences at $p < 0.05$ and $p < 0.001$, respectively. **(C)** Survival rates of mice with *E. coli* induced meningitis as a function of time up to 18 days after initiating treatment. Differences between groups were analyzed using log-ranking. * and *** indicate significant differences at $p < 0.05$ and $p < 0.001$, respectively. **(D)** *E. coli* CFUs in homogenized brain tissue from mice sacrificed 2 days after initiating treatment. Data represent means ± SDs over 6 mice per group. Differences between groups were analyzed using one-way ANOVA. *** indicate significant differences at $p < 0.001$. **(E)** *E. coli* CFUs in homogenized brain tissue from mice sacrificed at day 18, i.e. 14 days after arresting treatment. Data represent means ± SDs over 5 mice per group. Differences between groups were analyzed using one-way ANOVA. * and *** indicate significant differences at $p < 0.05$ and $p < 0.001$, respectively. **(F)** Histological images of hematoxylin and eosin stained sections of ventricular and meningeal outer regions of the brain, collected from 3 mice sacrificed 2 days after initiating treatment. Infiltrating neutrophils and erythrocytes are indicated by black and red arrows, respectively. **(G)** Same as panel f, now showing TUNEL-stained brain sections, with neuronal damage indicated by black arrows.

the brain, OMVs are also able to slowly diffuse out of the brain over a time course of 24 h, without magnetic field assistance. Secondly, sonodynamically-induced generation of ROS combined with CRO release provides a dual attack against which CRO-tolerant bacteria appeared to have no defence. Also in other applications, traditional antibiotic treatments could be made effective against antibiotic-tolerant or antibiotic-resistant pathogens by combination of ROS with an antibiotic [46–48].

ROS has a range of bacterial targets, including DNA, RNA, lipids, proteins and cell membranes and does not require uptake in growing bacteria as many antibiotics do [49]. ROS provides synergistic action with CRO by creating easier access of CRO into a bacterium, while intra-bacterial presence of CRO alters the redox state within bacteria and enhances intra-bacterial accumulation of ROS [49,50], which inhibits peptidoglycan synthesis [51]. The short lifetime of ROS in the order of several micro-seconds, allows it to diffuse over only very short distances of around 200 nm in aqueous solutions [52]. This makes the timing of ultrasound application for the sonodynamic induction of ROS generation crucial and ultrasound application should occur not only after OMVs have been magnetically driven across the blood-brain barrier, but also after sufficient time has been provided for the OMV to fuse into infecting pathogens.

The main limiting factor of this study with regards to further human clinical translation is the extrapolation of our conclusions from the relatively small volume of the murine brain to the much larger human brain and a thicker human skull. The current ultrasound conditions were chosen to have a relatively low frequency (40 kHz) to ensure good penetration in the brain, but the low frequency bears the risk of cavitation, thermal effects and associated intracerebral hemorrhage [53–55]. However, no signs of intracerebral hemorrhage or other types of brain damage (Fig. 6B, **F** and **G**) were observed, probably due to the use of a relatively low ultrasound power (intensity 2 W/cm^2) and short duration (5 min at 50% duty cycle). For comparison, focused ultrasound treatment is usually done at frequencies ranging from 1 to 7 MHz [56]. In diagnostic ultrasound application, high intensities are considered to range between 1000 and 10000 W/cm^2), while low intensities are described as < 3 W/cm^2 [33]. Thus, the ultrasound conditions applied here may be considered safe. However, specific guidelines for safe brain treatment are still emerging. Future human clinical use of magnetically-targetable OMVs will undoubtedly be done using more powerful magnetic targeting technologies based on 3D multi-magnet systems [57], providing better targeting precision within shorter periods of magnetic field application.

In summary (see also Fig. 7), we have demonstrated how non-inflammatory, magnetic OMVs can be driven over the blood-brain barrier by an external magnetic field. When loaded with a combination of CRO and TCPP, ultrasound application yielded ROS generation by TCPP that worked synergistically with CRO in the treatment of bacterially-induced meningitis in mice. Effective sonodynamic treatment could already be initiated within 3 h after magnetically driving the OMVs across the blood-brain barrier, which is clinically highly important considering the speed at which acute meningitis can result in death. Recurrence of meningitis remained absent for at least two weeks after arresting treatment despite the use of a CRO-tolerant pathogen, while OMVs accumulated in the brain diffused slowly out of the brain and were removed from the body through the urinary tract. We believe that we have provided proof-of-principle of a novel, direly needed strategy for the treatment of acute, bacterial meningitis that warrants further clinical translation.

4. Materials and methods

4.1. Materials

All chemicals purchased were analytical grade and used without further purification. Oleic acid (90%), oleyl amine, 1,2-dexadecanediol (97%), benzyl ether (99%), iron acetylacetonate (Fe(acac)$_3$), cacodylate buffer, acetonitrile, trifluoroacetic acid and DCFH-DA probes were purchased from Sigma-Aldrich (Beijing, China). Ethanol was purchased from Sinopharm Chemical Reagent Co., Ltd. (Shanghai, China). SYTO9/propidium iodide (Live/Dead Viability Kit) and DAPI were purchased from Thermo Fisher Scientific (Beijing, China). Glutaraldehyde and

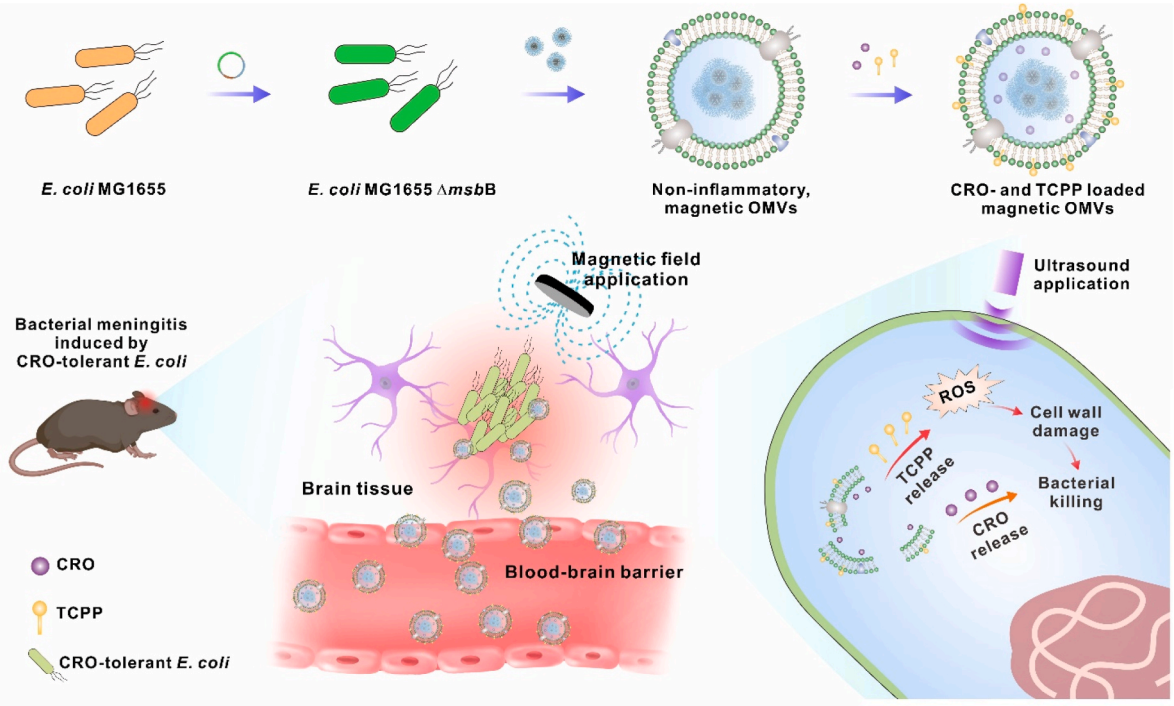

Fig. 7. Summarizing, schematic diagram of the full research presented, resulting in the killing of bacterial pathogens in the brain by synergistic action between ROS generation and CRO release.

tetrahydrofuran (THF) were purchased from J&K Scientific Ltd. (Shanghai, China). Sodium chloride (NaCl), potassium chloride (KCl), Na_2HPO_4, and KH_2PO_4, were purchased from Chemical Industrial Co. (Shanghai, China). The 2,5-dihydroxybenzoic acid was purchased from Bruker (Billerica, Massachusetts, USA). Ethylenediaminetetraacetic acid (EDTA) was purchased from MERYER Co., Ltd. (Shanghai, China). Tetrakis (4-carboxyphenyl) porphyrin (TCPP) was bought from TCI Co., Ltd. (Shanghai, China). Uranyl acetate was obtained from HEAD Biotechnology Co., Ltd. (Beijing, China). Ceftriaxone (CRO) was purchased from Shanghai Yuanye Bio-Technology Co., Ltd. (Shanghai, China). Singlet oxygen sensor green (SOSG) was purchased from Beyotime (Shanghai, China). Enzyme-linked immunosorbent assay (ELISA) kits for IL-6 and anti-CD31 antibodies were obtained from Abcam (Cambridge, UK), and ELISA kit for TNF-α was obtained from Beyotime Biotechnology (Shanghai, China). Luria-Bertani (LB) from Microbial Reagent Co. Ltd. (Hangzhou, China). Ultrapure water (Millipore Milli-Q grade, 18.2 MΩ) was used in all experiments.

4.2. Bacterial strain selection and construction, culturing and harvesting

E. coli ATCC 25922 and *E. coli* MG1655 (ATCC 700926) were obtained from the American Type Culture Collection (Baltimore, USA) and have been used before for magnetic outer-membrane vesicle (OMV) harvesting [26]. In order to construct a msbB deletion mutant of *E. coli* MG1655 (*E. coli* MG1655 Δ*msbB*), in which lipid A acyltransferase synthesis was inhibited, CRISPR/Cas9 gene knockout was employed [29]. First, the primers were designed and the upstream homologous arm (with ~580 bp-length) and the downstream homologous arm (with ~560 bp-length) of the target gene (*msbB*) were obtained by PCR amplification. Then the upstream homologous arm and downstream homologous arm were fused by extension PCR. Subsequently, the fusion fragment was connected with the T-vector and transferred into the receptive state of *E. coli* MG1655 along with CRISPR/Cas9 knockout plasmids by electroporation. After the knockout of *msbB*, the gene was extracted and knock-out verified by PCR amplification.

A CRO-tolerant *E. coli* ATCC 25922 mutant was constructed by cyclic exposure to ceftriaxone (CRO) [35]. First, an overnight culture (0.5 mL; 5×10^8 bacteria/mL) was diluted 1:100 into 50 mL Luria-Bertani (LB) growth medium supplemented with 2.5 μg/mL (>MIC x 10) CRO and incubated at 37 °C for 3 h with shaking at 220 rpm. Next, the CRO-containing medium was removed by centrifugation for 5 min at 4000×*g* and bacteria were washed twice in LB medium. Subsequently, bacteria were resuspended in 1 mL fresh LB medium for overnight culture. This procedure was repeated 5 times after which the minimal inhibitory concentration (MIC) and minimum bactericidal concentration (MBC) values together with the minimum duration for killing 99% of all bacteria (MDK_{99}) were determined.

All *E. coli* strains were kept on LB agar plates, pre-cultured in LB medium for 24 h at 37 °C in ambient air and finally cultured for another 16 h. Harvesting was done by centrifugation for 5 min at 4000 x g, followed by washing (2×) in phosphate-buffered saline (PBS; NaCl: 0.137 M, KCl: 0.0027 M, Na_2HPO_4: 0.01 M, KH_2PO_4: 0.0018 M, pH 7.4) and suspended in LB medium to concentrations appropriate to the respective experiments, as determined by colony forming units (CFU) enumeration on LB agar plates.

4.3. Preparation of OMVs and drug loading

OMVs were harvested as previously reported [26]. First, magnetic nanoparticles were prepared. To this end, 2 mmol $Fe(acac)_3$, 10 mmol 1, 2-dexadecanediol, 6 mmol oleic acid, 6 mmol oleyl amine, and 20 mL benzyl ether were mixed, and kept at 200 °C for 2 h, and subsequently heated to 300 °C for 1 h under nitrogen gas. The mixture was cooled down to room temperature and washed with 100% ethanol. Magnetic nanoparticles were obtained by centrifugation (21000 g, 10 min) and resuspended in tetrahydrofuran for PEGylation to improve their water suspendability and facilitate bacterial uptake.

Subsequently, *E. coli* MG1655 Δ*msbB* was grown as described above, but now in presence of magnetic nanoparticles (200 μg/mL) [26]. After bacterial growth for 24 h, the suspension was centrifuged and pelleted bacteria were transferred to fresh growth medium without magnetic nanoparticles and culturing was continued for another 24 h. After centrifugation and filtration, OMVs were magnetically harvested and resuspended in PBS.

For CRO loading into OMVs, purified OMVs (0.5 mg OMV protein/mL in PBS) were first mixed with different concentrations of CRO in PBS at room temperature. Then the mixture was sonicated using a BILON92-II Probe Sonicator (Shanghai Bilon Instrument Co., Ltd., China) with the following settings: 40 W, 8 cycles of 20 s on/off with a 90 s cooling period between each cycle. During sonication, cavitation occurs in the suspension fluid. The collapse of cavitation bubbles near an OMV generates a microstream that propels the CRO into an OMV, while possible damage to the OMVs is restored by self-re-assembly of the OMV membrane [58]. After sonication, the mixture was incubated at 37 °C for 60 min to stabilize the OMV membranes. Excess free CRO was separated from the CRO-loaded OMVs by magnetic separation. For TCPP loading, CRO-loaded OMVs were mixed with different concentrations of TCPP and incubated at 37 °C for 1 h during which TCPP, due to its hydrophobicity, will distribute in the lipid bilayer of an OMV and diffuse inwards [58]. Subsequently, dual-drug loaded OMVs were magnetically separated.

Drug loading was determined using MALDI-TOF MS. Briefly, drug-loaded OMVs were suspended in PBS and deposited on a MALDI target plate (MSP 384 ground steel target, Bruker Daltonics, German) by drop casting (1 μL for each spot) and air-dried for 15 min. 2,5-Dihydroxybenzoic acid (20 mg/mL) was dissolved in acetonitrile/water/trifluoroacetic acid (volume percentage, 50/49.9/0.1%) solution and used as a matrix. MALDI-TOF MS was performed on a Bruker BIFLEX III mass spectrometer (Bruker Daltonics, Germany) equipped with an Nd:YAG laser (wavelength 355 nm, laser pulse duration 3 ns) with reflection in positive-ion modes. The amount of drug-loaded into OMVs was measured by a UV–vis spectrophotometer (NanoDrop, Thermo Fisher Scientific) after disintegrating the drug-loaded OMVs using 0.1 M EDTA (pH 8.0) for 1 h at 37 °C. Absorbance wavelengths of 254 nm and 414 nm were used for CRO and TCPP, respectively and after making a calibration curve for CRO and TCPP (Fig. S3), drug loading efficiencies were calculated according to

$$\text{Drug Loading effiency} = \frac{\text{weight of TCPP or CRO loaded}}{\text{total protein weight of OMVs}} \times 100\%$$

4.4. Characterization of OMVs

Zeta potentials and hydrodynamic diameters of OMVs with or without drug-loading were measured in PBS at 25 °C using a Zetasizer Nano ZS (Malvern Instruments, UK). For transmission electron microscopy (TEM) and high-angle annular dark-field scanning TEM (HAADF-STEM), OMVs were fixed in 2.5% glutaraldehyde in cacodylate buffer (pH 7.4, 0.1 M) at 4 °C for 1 h and 5 μL droplets were placed onto a carbon-coated copper grid and allowed to attach for 20 min. Grids were washed in cacodylate buffer (pH 7.4, 0.1 M) and stained with 2% uranyl acetate. After removing the excess stain, grids were rinsed with water, air-dried at room temperature, and examined on a Tecnai F20 microscope operated at 120 kV (FEI, USA).

4.5. CRO- and TCPP-release from OMVs upon ultrasound application

Release of CRO and TCPP from the CRO- and TCPP-loaded OMVs was determined using dialysis in absence and presence of ultrasound application (1 mL OMV suspension at 40 kHz, 2 W/cm^2, 50% duty cycle). These ultrasound conditions are common in sonodynamic treatments and can be applied maximally a few minutes, possibly ranging up to 30

min, depending on the treatment goal [59]. For the current treatment goal involving brain tissue longer duration times are not advisable and hence ultrasound treatment was done for 5 min. After ultrasound application, sonicated OMVs were added to a dialysis bag (molecular weight cut-off at 3500, Shanghai Yuanye Biotechnology Corporation, Shanghai, China) and dialysis was carried out against 30 mL PBS, pH 7.4 in the dark at 37 °C. After 1, 4, 8, and 12 h, 500 μL of dialysate was collected and the amounts of CRO and TCPP released from the OMVs were quantified by UV–vis spectrophotometer (see above) using a calibration curve (Fig. S3), after concentrating the OMV suspension by centrifugation when needed in order to measure concentrations within the range of the calibration curve. After taking aliquots, 500 μL of PBS was added to ensure a constant volume.

4.6. Quantification of ROS generation by ultrasonication of TCPP

TCPP in solution or CRO- and TCPP-loaded OMVs in PBS at a TCPP equivalent concentration of 2 μg/mL were mixed with a commercially obtained Reactive Oxygen Species (ROS) probe, singlet oxygen sensor green (SOSG, 0.5 mM), and ultrasonicated (40 kHz, 2 W/cm^2, 50% duty cycle; Suzhou Nathan Ultrasonic Technology Co., Suzhou, China) for 2, 5 and 10 min. Subsequently, the fluorescence of each sample was detected using a microplate reader (Variskan, Thermo Fisher Scientific, Waltham, USA) at excitation and emission wavelengths of 488 and 525 nm, respectively.

4.7. Efficacy of CRO- and TCPP-loaded OMVs against CRO-tolerant *E. coli* in vitro

The killing efficacy of CRO- and TCPP-loaded OMVs towards planktonic, CRO-tolerant *E. coli* ATCC 25922 was determined by suspending bacteria (5×10^6 CFU/mL) in PBS and mixing with equal volumes with suspensions of CRO-loaded OMVs, TCPP-loaded OMVs, or CRO- and TCPP-loaded OMVs at CRO and TCPP equivalent concentrations of 2 μg/mL and 0.4 μg/mL, respectively. After incubation for 2.5 h in the dark, the suspension was ultrasonicated (40 kHz, 2 W/cm^2, 50% duty cycle) for 5 min and centrifuged to re-suspended in PBS. 10 μL aliquots were taken from each suspension, serially diluted, and plated on LB agar plates. After 24 h at 37 °C in ambient air, the number of CFUs was counted. Also, possible cell membrane damage was assessed using SYTO9/propidium iodide staining, turning green-fluorescent bacteria with an intact cell membrane into red-fluorescent ones in case of cell wall damage. Levels of ROS generated in the bacteria were assessed using a green-fluorescence ROS probe, 2,7-dichlorodihydrofluorescein diacetate (DCFH-DA). To this end, *E. coli* were stained with 10 μM DCFH-DA and left in the dark for 20 min at 37 °C prior to OMV exposure and ultrasonication (40 kHz, 2 W/cm^2, 50% duty cycle) for 5 min and immediately imaged using confocal laser scanning microscopy (CLSM; Zeiss confocal microscope, equipped with a 63× objective lens).

4.8. Animals and induction of meningitis

Female C57BL/6 mice were purchased from Changzhou Cavens Experimental Animal Co. Ltd. All animal experiments were performed in compliance with the relevant laws and approved by the Institutional Animal Care and User's Committee of Soochow University (approval number 202112A0217). Acute bacterial meningitis by CRO-tolerant *E. coli* was induced using a method previously established for inducing meningitis by *Streptococcus pneumoniae* in mice [38]. After anesthesia (intraperitoneal injection of chloral hydrate 5%, v/v), mice were immobilized on a stereotaxic device and 10 μL of a CRO-tolerant *E. coli* ATCC 25922 suspension (1×10^7 CFU/mL) was inoculated by the intracranial route through a soft point located along the skull midline, 3.5 mm rostral to the bregma, yielding a dose of 1×10^5 CFU per site.

4.9. Inflammation upon OMV injection in mice

In order to study possible short-term signs of inflammation upon OMV injection in mice, serum cytokine concentrations were measured in healthy mice 6 h after initial intravenous injection in the tail with 100 μL PBS, *E. coli* MG1655 or *E. coli* MG1655 Δ*msbB* derived magnetic OMVs. OMVs were administered to yield doses of 0.6, 6 or 60 mg/kg. Blood was collected through the eye from mice surviving at 6 h post-injection, i.e. mice injected with a dose of 0.6 mg/kg and allowed to clot at room temperature for 30 min. Samples were then centrifuged at 800 x g for 10 min to collect serum from the supernatant. Il-6 and TNF-α concentrations were measured using commercially available ELISA kits following the manufacturer's instructions.

In order to evaluate biosafety of OMV injection, twelve healthy mice were divided randomly in 4 groups that were intravenously injected in the tail with CRO- and TCPP-loaded OMVs or PBS on day 1, day 9 and day 15. Mice were sacrificed one day after each injection and main organs of mice collected to conduct the hematoxylin and eosin (H and E) staining of excised tissue. Blood and serum samples were collected for blood biochemistry analysis.

4.10. Magnetically-driving OMVs across the blood-brain barrier in mice

Healthy mice were intravenously injected in the tail with a single injection of TCPP in PBS or CRO- and TCPP-loaded OMVs at a TCPP equivalent dose of 10 mg/kg in absence and presence of magnetic field application. For magnetically driving the OMVs across the blood-brain barrier, a magnet (0.3 T, 10 mm x 10 mm) was placed over the head lesion area of the mice and fixed with medical tape. For bio-optical imaging, mice were anesthetized with 2.5% isoflurane (RWD Life Sciences, China) at each selected time point and the TCPP fluorescence in the head area of the mouse was imaged using the IVIS Lumina III Imaging System (PerkinElmer, image acquisition factors: 0.5 s exposure time, emission wavelength 600 nm, excitation wavelength 710 nm). Images were automatically corrected for background noise and were analyzed using Living Image software (PerkinElmer).

In order to determine the distribution of OMVs in the brain (and other organs), mice were sacrificed 3 h and 24 h after tail-vein injection of OMVs. After excision of the liver, spleen, lungs, kidneys and brain, brain tissue was fixed in 4% paraformaldehyde for 12 h, frozen and sectioned. Immunofluorescence vasculature and nucleus staining was applied on the brain tissue excised using anti-CD31 and DAPI, respectively and brain sections imaged using CLSM (Zeiss CLSM 800, Germany). Fluorescence intensities were quantitated using built-in software (Zen 2011, Jena, Germany) of the CLSM. All excised tissue of primary organs was weighted and homogenized in 1 mL PBS. Supernatants were obtained by centrifugation at 10,000 g for 10 min and TCPP concentrations recorded using a microplate reader (Variskan, Thermo Fisher Scientific, Waltham, USA).

4.11. Treatment of bacterial meningitis in mice

Treatment was started 12 h after initiating infection. Infected mice were treated at 09.00 a.m. on four consecutive days, including day 0 with PBS, CRO free in solution and CRO- and TCPP-loaded OMVs with or without magnetic field and/or ultrasound application (5 min, 40 kHz, 2 W/cm^2, 50% duty cycle) all at CRO and TCPP equivalent doses of 50 mg/kg and 10 mg/kg, respectively. Behavior of the mice was scored every 12 h, starting at 08.00 a.m. on day 0, according to a clinically applied protocol [60,61] by an observer, uninformed about the treatment protocol of individual mice. Score 0 indicates no apparent behavioral abnormality, score 1 indicates moderate lethargy (apparent decrease of spontaneous activity), score 2 indicates severe lethargy (rare spontaneous movements, but walking after stimulation by the investigator), score 3 indicates unability to walk and score 4 indicates death. Mice with clinical scores of 3 were sacrificed for ethical reasons.

The number of bacterial CFUs in brain tissue of surviving mice were determined after sacrifice at day 2 after initiating treatment and day 18, i.e. 14 days after arresting treatment. To this end, mice were sacrificed, brains were excised and weighted, brain tissue was homogenized in PBS and serial dilutions were plated on blood-agar plates for enumeration after 48 h incubation at 37 °C. Histology on brain sections taken at day 2 after initiating treatment was performed after H and E (Servicebio, Wuhan, China) and TUNEL (Servicebio, Wuhan, China) staining. To this end, excised brain tissue was fixed overnight in 4% paraformaldehyde and embedded in paraffin. Paraffin-embedded brain tissues were sectioned coronally (4–6 μm thick sections) using a microtome prior to staining, according to the respective manufacturer's instructions.

4.12. Statistical analysis

All data were expressed as means ± standard deviations (SDs). For statistical evaluation, GraphPad Prism (8.3.0) was used. Differences between two groups were analyzed using a Student's t-test. Multivariate parametric data were examined using one-way ANOVA with Tukey's post hoc comparison. Differences were considered significant at $p < 0.05$.

Credit author statement

RS, HCvdM, JL, and HJB designed experiments. RS, RL, ZD, QC, RW, and SL performed experiments. RS and HJB wrote the manuscript. YR, HJB, HCvdM, and JL edited the manuscript. All the authors analyzed the data and contributed to the paper.

Funding

This work was financially supported by the National Key Research and Development Program of China (2017YFE0131700), China; the National Natural Science Foundation of China (21874096), China; the 111 Project, China; Joint International Research Laboratory of Carbon-Based Materials and Devices, China; the Collaborative Innovation Center of Suzhou Nano Science and Technology, China; Suzhou Key Laboratory of Nanotechnology and Biomedicine, China; and UMCG, Groningen, The Netherlands.

Data and materials availability

The data that support the findings of this study are available from the corresponding authors upon request.

Declaration of competing interest

The authors declare the following financial interests/personal relationships which may be considered as potential competing interests: HJB is also director of a consulting company, SASA BV (GN Schutterlaan 4, 9797 PC Thesinge, The Netherlands). The authors declare no potential conflicts of interest with respect to authorship and/or publication of this article.

Data availability

Data will be made available on request.

Appendix A. Supplementary data

Supplementary data to this article can be found online at https://doi.org/10.1016/j.biomaterials.2023.122320.

References

[1] C. Kietzman, E. Tuomanen, Acute bacterial meningitis: challenges to better antibiotic therapy, ACS Infect. Dis. 5 (2019) 1987–1995.
[2] D. van de Beek, M. Brouwer, R. Hasbun, U. Koedel, C.G. Whitney, E. Wijdicks, Community-acquired bacterial meningitis, Nat. Rev. Dis. Prim. 2 (2016), 16074.
[3] E.C. Wall, J.M. Chan, E. Gil, R.S. Heyderman, Acute bacterial meningitis, Curr. Opin. Neurol. 34 (2021) 386–395.
[4] J.L. Bradshaw, L.S. McDaniel, Selective pressure: rise of the nonencapsulated pneumococcus, PLoS Pathog. 15 (2019), e1007911.
[5] F. McGill, R.S. Heyderman, S. Panagiotou, A.R. Tunkel, T. Solomon, Acute bacterial meningitis in adults, Lancet 388 (2016) 3036–3047.
[6] E. Martinez, A. Marcos, Acute bacterial meningitis in adults, N. Engl. J. Med. 328 (1993) 1712–1713.
[7] E.H. Price, J. de Louvois, M.R. Workman, Antibiotics for *Salmonella meningitis* in children, J. Antimicrob. Chemother. 46 (2000) 653–655.
[8] E. Nance, S.H. Pun, R. Saigal, D.L. Sellers, Drug delivery to the central nervous system, Nat. Rev. Mater. 7 (2021) 314–331.
[9] R. Pandit, L. Chen, J. Gotz, The blood-brain barrier: physiology and strategies for drug delivery, Adv. Drug Deliv. Rev. 165–166 (2020) 1–14.
[10] J.V. Forrester, P.G. McMenamin, S.J. Dando, CNS infection and immune privilege, Nat. Rev. Neurosci. 19 (2018) 655–671.
[11] J.A. Aarli, The immune system and the nervous system, J. Neurol. 229 (1983) 137–154.
[12] A. Brauner, O. Fridman, O. Gefen, N.Q. Balaban, Distinguishing between resistance, tolerance and persistence to antibiotic treatment, Nat. Rev. Microbiol. 14 (2016) 320–330.
[13] I. Levin-Reisman, I. Ronin, O. Gefen, I. Braniss, N. Shoresh, N.Q. Balaban, Antibiotic tolerance facilitates the evolution of resistance, Science 355 (2017) 826–830.
[14] E. Tuomanen, D.T. Durack, A. Tomasz, Antibiotic tolerance among clinical isolates of bacteria, Antimicrob. Agents Chemother. 30 (1986) 521–527.
[15] E. Tuomanen, H. Pollack, A. Parkinson, M. Davidson, R. Facklam, R. Rich, O. Zak, Microbiological and clinical significance of a new property of defective lysis in clinical strains of pneumococci, J. Infect. Dis. 158 (1988) 36–43.
[16] F. Ciummo, P. Srinivas, J. Biedny, Antimicrobial use in central nervous system infections, Curr. Opin. Infect. Dis. 34 (2021) 255–263.
[17] E. Carter, F. McGill, The management of acute meningitis: an update, Clin. Med. 22 (2022) 396–400.
[18] D. Sun, X. Pang, Y. Cheng, J. Ming, S. Xiang, C. Zhang, P. Lv, C. Chu, X. Chen, G. Liu, N. Zheng, Ultrasound-switchable nanozyme augments sonodynamic therapy against multidrug-resistant bacterial infection, ACS Nano 14 (2020) 2063–2076.
[19] D. Costley, H. Nesbitt, N. Ternan, J. Dooley, Y.Y. Huang, M.R. Hamblin, A. P. McHale, J.F. Callan, Sonodynamic inactivation of Gram-positive and Gram-negative bacteria using a Rose Bengal-antimicrobial peptide conjugate, Int. J. Antimicrob. Agents 49 (2017) 31–36.
[20] Y. Zhang, X. Zhang, H. Yang, L. Yu, Y. Xu, A. Sharma, P. Yin, X. Li, J.S. Kim, Y. Sun, Advanced biotechnology-assisted precise sonodynamic therapy, Chem. Soc. Rev. 50 (2021) 11227–11248.
[21] J. Roy, V. Pandey, I. Gupta, H. Shekhar, Antibacterial sonodynamic therapy: current status and future perspectives, ACS Biomater. Sci. Eng. 7 (2021) 5326–5338.
[22] D. Wang, D.B. Cheng, L. Ji, L.J. Niu, X.H. Zhang, Y. Cong, R.H. Cao, L. Zhou, F. Bai, Z.Y. Qiao, H. Wang, Precise magnetic resonance imaging-guided sonodynamic therapy for drug-resistant bacterial deep infection, Biomaterials 264 (2021), 120386.
[23] A. Kulp, M.J. Kuehn, Biological functions and biogenesis of secreted bacterial outer membrane vesicles, Annu. Rev. Microbiol. 64 (2010) 163–184.
[24] C. Schwechheimer, M.J. Kuehn, Outer-membrane vesicles from Gram-negative bacteria: biogenesis and functions, Nat. Rev. Microbiol. 13 (2015) 605–619.
[25] O.Y. Kim, H.T. Park, N.T.H. Dinh, S.J. Choi, J. Lee, J.H. Kim, S.W. Lee, Y.S. Gho, Bacterial outer membrane vesicles suppress tumor by interferon-gamma-mediated antitumor response, Nat. Commun. 8 (2017) 626.
[26] R. Shi, Z. Dong, C. Ma, R. Wu, R. Lv, S. Liu, Y. Ren, Z. Liu, H.C. van der Mei, H. J. Busscher, J. Liu, High-yield, magnetic harvesting of extracellular outer-membrane vesicles from *Escherichia coli*, Small 18 (2022), e2204350.
[27] M. Li, H. Zhou, C. Yang, Y. Wu, X. Zhou, H. Liu, Y. Wang, Bacterial outer membrane vesicles as a platform for biomedical applications: an update, J. Contr. Release 323 (2020) 253–268.
[28] Q. Chen, H. Bai, W. Wu, G. Huang, Y. Li, M. Wu, G. Tang, Y. Ping, Bioengineering bacterial vesicle-coated polymeric nanomedicine for enhanced cancer immunotherapy and metastasis prevention, Nano Lett. 20 (2020) 11–21.
[29] Q. Guo, X. Li, W. Zhou, Y. Chu, Q. Chen, Y. Zhang, C. Li, H. Chen, P. Liu, Z. Zhao, Y. Wang, Z. Zhou, Y. Luo, C. Li, H. You, H. Song, B. Su, T. Zhang, T. Sun, C. Jiang, Sequentially triggered bacterial outer membrane vesicles for macrophage metabolism modulation and tumor metastasis suppression, ACS Nano 15 (2021) 13826–13838.
[30] M.A. Jhonsi, R. Renganathan, Investigations on the photoinduced interaction of water soluble thioglycolic acid (TGA) capped CdTe quantum dots with certain porphyrins, J. Colloid Interface Sci. 344 (2010) 596–602.
[31] S.W. Kim, S.B. Park, S.P. Im, J.S. Lee, J.W. Jung, T.W. Gong, J.M.S. Lazarte, J. Kim, J.S. Seo, J.H. Kim, J.W. Song, H.S. Jung, G.J. Kim, Y.J. Lee, S.K. Lim, T.S. Jung, Outer membrane vesicles from beta-lactam-resistant *Escherichia coli* enable the survival of beta-lactam-susceptible *E. coli* in the presence of beta-lactam antibiotics, Sci. Rep. 8 (2018) 5402.

[32] A. Schroeder, J. Kost, Y. Barenholz, Ultrasound, liposomes, and drug delivery: principles for using ultrasound to control the release of drugs from liposomes, Chem. Phys. Lipids 162 (2009) 1–16.
[33] V.S. Bachu, J. Kedda, I. Suk, J.J. Green, B. Tyler, High-intensity focused ultrasound: a review of mechanisms and clinical applications, Ann. Biomed. Eng. 49 (2021) 1975–1991.
[34] Z. Dong, L. Feng, Y. Hao, Q. Li, M. Chen, Z. Yang, H. Zhao, Z. Liu, Synthesis of CaCO3-based nanomedicine for enhanced sonodynamic therapy via amplification of tumor oxidative stress, Chem 6 (2020) 1391–1407.
[35] O. Fridman, A. Goldberg, I. Ronin, N. Shoresh, N.Q. Balaban, Optimization of lag time underlies antibiotic tolerance in evolved bacterial populations, Nature 513 (2014) 418–421.
[36] G. Jiang, S. Liu, T. Yu, R. Wu, Y. Ren, H.C. van der Mei, J. Liu, H.J. Busscher, PAMAM dendrimers with dual-conjugated vancomycin and Ag-nanoparticles do not induce bacterial resistance and kill vancomycin-resistant Staphylococci, Acta Biomater. 123 (2021) 230–243.
[37] A. Mulhall, J. de Louvois, J. James, Pharmacokinetics and safety of ceftriaxone in the neonate, Eur. J. Pediatr. 144 (1985) 379–382.
[38] D. Chiavolini, S. Tripodi, R. Parigi, M.R. Oggioni, E. Blasi, M. Cintorino, G. Pozzi, S. Ricci, Method for inducing experimental pneumococcal meningitis in outbred mice, BMC Microbiol. 4 (2004) 36.
[39] H.J. Busscher, W. Woudstra, T.G. van Kooten, P. Jutte, L. Shi, J. Liu, W.L. J. Hinrichs, H.W. Frijlink, R. Shi, J. Liu, J. Parvizi, S. Kates, V.M. Rotello, T. P. Schaer, D. Williams, D.W. Grainger, H.C. van der Mei, Accepting higher morbidity in exchange for sacrificing fewer animals in studies developing novel infection-control strategies, Biomaterials 232 (2020), 119737.
[40] S.R. Coats, C.T. Do, L.M. Karimi-Naser, P.H. Braham, R.P. Darveau, Antagonistic lipopolysaccharides block *E. coli* lipopolysaccharide function at human TLR4 via interaction with the human MD-2 lipopolysaccharide binding site, Cell Microbiol. 9 (2007) 1191–1202.
[41] J.E. Somerville Jr., L. Cassiano, B. Bainbridge, M.D. Cunningham, R.P. Darveau, A novel *Escherichia coli* lipid A mutant that produces an antiinflammatory lipopolysaccharide, J. Clin. Invest. 97 (1996) 359–365.
[42] T. Mainprize, N. Lipsman, Y. Huang, Y. Meng, A. Bethune, S. Ironside, C. Heyn, R. Alkins, M. Trudeau, A. Sahgal, J. Perry, K. Hynynen, Blood-brain barrier opening in primary brain tumors with non-invasive MR-guided focused ultrasound: a clinical safety and feasibility study, Sci. Rep. 9 (2019) 321.
[43] T. Yin, L. Yang, Y. Liu, X. Zhou, J. Sun, J. Liu, Sialic acid (SA)-modified selenium nanoparticles coated with a high blood-brain barrier permeability peptide-B6 peptide for potential use in Alzheimer's disease, Acta Biomater. 25 (2015) 172–183.
[44] Y. Na, N. Zhang, X. Zhong, J. Gu, C. Yan, S. Yin, X. Lei, J. Zhao, F. Geng, Polylactic-co-glycolic acid-based nanoparticles modified with peptides and other linkers cross the blood-brain barrier for targeted drug delivery, Nanomedicine 18 (2023) 125–143.
[45] W. Xiao, Y. Wang, H. Zhang, Y. Liu, R. Xie, X. He, Y. Zhou, L. Liang, H. Gao, The protein corona hampers the transcytosis of transferrin-modified nanoparticles through blood-brain barrier and attenuates their targeting ability to brain tumor, Biomaterials 274 (2021), 120888.
[46] C.M. Courtney, S.M. Goodman, T.A. Nagy, M. Levy, P. Bhusal, N.E. Madinger, C. S. Detweiler, P. Nagpal, A. Chatterjee, Potentiating antibiotics in drug-resistant clinical isolates via stimuli-activated superoxide generation, Sci. Adv. 3 (2017), e1701776.
[47] Y. Liu, Y. Jia, K. Yang, Z. Tong, J. Shi, R. Li, X. Xiao, W. Ren, R. Hardeland, R. J. Reiter, Z. Wang, Melatonin overcomes MCR-mediated colistin resistance in Gram-negative pathogens, Theranostics 10 (2020) 10697–10711.
[48] A. Arce-Rodriguez, D. Pankratz, M. Preusse, P.I. Nikel, S. Haussler, Dual effect: high NADH levels contribute to efflux-mediated antibiotic resistance but drive lethality mediated by reactive oxygen species, Bio 13 (2022), e0243421.
[49] Y. Hong, J. Zeng, X. Wang, K. Drlica, X. Zhao, Post-stress bacterial cell death mediated by reactive oxygen species, Proc. Natl. Acad. Sci. USA 116 (2019) 10064–10071.
[50] D.J. Dwyer, P.A. Belenky, J.H. Yang, I.C. MacDonald, J.D. Martell, N. Takahashi, C. T. Chan, M.A. Lobritz, D. Braff, E.G. Schwarz, J.D. Ye, M. Pati, M. Vercruysse, P. S. Ralifo, K.R. Allison, A.S. Khalil, A.Y. Ting, G.C. Walker, J.J. Collins, Antibiotics induce redox-related physiological alterations as part of their lethality, Proc. Natl. Acad. Sci. USA 111 (2014) 2100–2109.
[51] A.A. Al kraiem, G. Yang, F. Al kraiem, T. Chen, Challenges associated with ceftriaxone resistance in Salmonella, Front. Life Sci. 11 (2018) 26–34.
[52] R.W. Redmond, I.E. Kochevar, Spatially resolved cellular responses to singlet oxygen, Photochem. Photobiol. 82 (2006) 1178–1186.
[53] C. Baron, J.F. Aubry, M. Tanter, S. Meairs, M. Fink, Simulation of intracranial acoustic fields in clinical trials of sonothrombolysis, Ultrasound Med. Biol. 35 (2009) 1148–1158.
[54] F. Ahmadi, I.V. McLoughlin, S. Chauhan, G. ter-Haar, Bio-effects and safety of low-intensity, low-frequency ultrasonic exposure, Prog. Biophys. Mol. Biol. 108 (2012) 119–138.
[55] G. ter Haar, A. Shaw, S. Pye, B. Ward, F. Bottomley, R. Nolan, A.M. Coady, Guidance on reporting ultrasound exposure conditions for bio-effects studies, Ultrasound Med. Biol. 37 (2011) 177–183.
[56] J.W. Jenne, T. Preusser, M. Gunther, High-intensity focused ultrasound: principles, therapy guidance, simulations and applications, Z. Med. Phys. 22 (2012) 311–322.
[57] X. Wang, Z. Gong, T. Wang, J. Law, X. Chen, S. Wanggou, J. Wang, B. Ying, M. Francisco, W. Dong, Y. Xiong, J.J. Fan, G. MacLeod, S. Angers, X. Li, P.B. Dirks, X. Liu, X. Huang, Y. Sun, Mechanical nanosurgery of chemoresistant glioblastoma using magnetically controlled carbon nanotubes, Sci. Adv. 9 (2023) eade5321.
[58] X.M. Xi, S.J. Xia, R. Lu, Drug loading techniques for exosome-based drug delivery systems, Pharmazie 76 (2021) 61–67.
[59] A. Lalzad, F. Wong, N. Singh, P. Coombs, C. Brockley, S. Brennan, M. Ditchfield, P. Rao, A. Watkins, V. Saxton, M. Schneider, Knowledge of safety, training, and practice of neonatal cranial ultrasound: a survey of operators, J. Ultrasound Med. 37 (2018) 1411–1421.
[60] S. Schutze, S. Ribes, A. Kaufmann, A. Manig, J. Scheffel, S. Redlich, S. Bunkowski, U.K. Hanisch, W. Bruck, R. Nau, Higher mortality and impaired elimination of bacteria in aged mice after intracerebral infection with *E. coli* are associated with an age-related decline of microglia and macrophage functions, Oncotarget 5 (2014) 12573–12592.
[61] G. Devraj, S. Guerit, J. Seele, D. Spitzer, J. Macas, M.I. Khel, R. Heidemann, A. K. Braczynski, W. Ballhorn, S. Gunther, O.O. Ogunshola, M. Mittelbronn, U. Kodel, C.M. Monoranu, K.H. Plate, S. Hammerschmidt, R. Nau, K. Devraj, V.A.J. Kempf, HIF-1alpha is involved in blood-brain barrier dysfunction and paracellular migration of bacteria in pneumococcal meningitis, Acta Neuropathol. 140 (2020) 183–208.